IEICE TRANS. COMMUN., VOL.E101–B, NO.3 MARCH 2018

PAPER

PTS-Based PAPR Reduction by Iterative p-Norm Minimization without Side Information in OFDM Systems

Moeko YOSHIDA[†*], ***Student Member***, **Hiromichi NASHIMOTO**[††], ***Nonmember***, ***and*** **Teruyuki MIYAJIMA**[†††a)], ***Member***

SUMMARY This paper proposes a partial transmit sequences (PTS)-based PAPR reduction method and a phase factor estimation method without side information for OFDM systems with QPSK and 16QAM modulation. In the transmitter, an iterative algorithm that minimizes the p-norm of a transmitted signal determines phase factors to reduce PAPR. Unlike conventional methods, the phase factors are allowed to take continuous values in a limited range. In the receiver, the phase factor is blindly estimated by evaluating the phase differences between the equalizer's output and its closest constellation points. Simulation results show that the proposed PAPR reduction method is more computationally efficient than the conventional PTS. Moreover, the combined use of the two proposed methods achieves a satisfactory tradeoff between PAPR and BER by limiting the phase factors properly.

key words: *OFDM, PAPR, PTS, adaptive algorithm, blind estimation*

1. Introduction

High peak-to-average power ratio (PAPR) is a major drawback of orthogonal frequency division multiplexing (OFDM) for high-speed wireless communications because it causes nonlinear distortion and low power efficiency at the transmitter power amplifier. Many researchers have proposed various PAPR reduction methods [1], [2], including clipping and filtering, tone reservation (TR) [3], and selective mapping (SLM) [4]. Among these methods, the partial transmit sequences (PTS) [5] has attracted a significant amount attention in the research community [6]–[15]. PTS, as well as SLM, does not cause a transmit power increase and signal distortion [1]. Also, PTS requires less amount of computation than SLM [2]. There are two disadvantages that we should overcome to make PTS practical: computational complexity increase due to phase factor optimization and data rate loss due to side information (SI) transmission.

In the conventional PTS [5], a data block is divided into resource blocks (RBs), and data symbols in an RB are rotated by a phase factor taking a discrete value in a finite set. Its PAPR reduction performance improves as either the number of possible values of phase factors and that of RBs increases. However, the optimization of phase factors requires an exhaustive search whose complexity increases exponentially with the number of RBs. To overcome the complexity issue, computationally efficient methods have been proposed. Their common idea is to find sub-optimum phase factors by reducing the search space [6], [7] or employing optimization algorithms [8]. In these methods using discrete-valued phase factors, complexity reduction can be achieved at the expense of PAPR reduction performance degradation.

Recently, it has been reported that the use of continuous-valued phase factors improves the performance as well as complexity reduction [9], [10]. A notable work in this line is [11] where an iterative method based on the constant modulus algorithm (CMA) optimizes the continuous-valued phase factors. This method achieves lower PAPR than the conventional PTS by a few iterations. As we show later, however, the CMA cost function is quite different from PAPR. The infinity norm of a transmitted signal, which can be equivalent to PAPR, may be a good candidate for a cost function as used in TR [16] and SLM [17]. However, it is also shown later that the infinity norm cost function is not suitable for PTS due to the existence of local minima. This suggests that it is worth exploring other cost functions.

Another issue of PTS is that the information of the phase factors is transmitted as SI for proper demodulation at the receiver. It results in not only data rate loss, but also BER degradation due to erroneous detection of SI. To overcome this issue, various methods without SI have been proposed. In [12], the information of phase factors is embedded in the transmitted signal. In [13], [14], maximum likelihood decoding is applied to recover the data symbols rotated by a modified phase factor. These methods exploit the discrete nature of phase factors, and cannot be applied to the PTS using continuous-valued phase factors. The methods in [10], [13], [15], which can be applied to the continuous-valued PTS, use pilot symbols inserted in each RB to estimate the corresponding phase factor. However, the pilot-based methods are impractical for the PTS with a number of RBs since the use of many pilot symbols reduces the effective data rate.

In this paper, we propose a computationally efficient PAPR reduction method where the continuous-valued phase factors are obtained by iteratively minimizing the p-norm cost function. Moreover, we propose a phase factor estimation method without SI and pilot symbols. By properly

Manuscript received November 7, 2016.
Manuscript revised May 29, 2017.
Manuscript publicized August 24, 2017.

[†]The author is with the Graduate School of Science and Engineering, Ibaraki University, Hitachi-shi, 316-8511 Japan.
[††]The author is with Nippon Signal Co. Ltd., Kuki-shi, 346-8524 Japan.
[†††]The author is with the Department of Electrical and Electronic Engineering, Ibaraki University, Hitachi-shi, 316-8511 Japan.
[*]Presently, with JVCKENWOOD Engineering Corp.
a) E-mail: teruyuki.miyajima.spc@vc.ibaraki.ac.jp

DOI: 10.1587/transcom.2016EBP3422

limiting the allowable range of phase factors without sacrifice of PAPR reduction performance, the phase factors can be successfully estimated and the resulting BER performance is satisfactory.

2. PTS-based OFDM System Model

2.1 Transmitter

We consider a PTS-based OFDM system with N subcarriers. Block diagram of the transmitter is shown in Fig. 1(a). A frequency-domain data block $\mathbf{d} = [d_1\ d_2\ \dots\ d_N]^T$ is partitioned into U RBs. The uth RB is represented by

$$\mathbf{s}_u = [s_{u,1}\ s_{u,2}\ \dots\ s_{u,N}]^T, \tag{1}$$

$$s_{u,n} = \begin{cases} d_n, & (u-1)N_b + 1 \le n \le uN_b \\ 0, & \text{otherwise} \end{cases} \tag{2}$$

where $N_b = N/U$ is the number of data symbols per RB. A time domain signal of length N is obtained by taking the inverse discrete Fourier transform (IDFT) of $\mathbf{s}_u$ as

$$\mathbf{x}_u = \mathbf{F}^H \mathbf{s}_u \tag{3}$$

where $\mathbf{F}$ denotes the N-point DFT matrix whose (k,l)th element is $\frac{\exp(-j2\pi(k-1)(l-1)/N)}{\sqrt{N}}$. At a PTS transmitter, we multiply the signal $\mathbf{x}_u$ by a phase factor $\omega_u = e^{j\theta_u}$ where θ_u is a phase coefficient. Then, a transmitted signal $\mathbf{x}$ is given by

$$\mathbf{x} = [x_1\ x_2\ \dots\ x_N]^T = \mathbf{A}\boldsymbol{\omega} = \mathbf{F}^H \mathbf{S}\boldsymbol{\omega} \tag{4}$$

where $\mathbf{A} = [\mathbf{x}_1\ \mathbf{x}_2\ \dots\ \mathbf{x}_U]$, $\boldsymbol{\omega} = [\omega_1\ \omega_2\ \dots\ \omega_U]^T$, and $\mathbf{S} = [\mathbf{s}_1\ \mathbf{s}_2\ \dots\ \mathbf{s}_U]$. This signal is transmitted after a cyclic prefix (CP) is added to the top of $\mathbf{x}$. The basic idea of PTS is to optimize the phase factors $\{\omega_u\}$ in (4) so as to minimize the PAPR of the transmitted signal, which is defined below.

To approximate the PAPR of a continuous-time transmitted signal, we consider an F_s times oversampled OFDM signal given by

$$\tilde{\mathbf{x}} = [\tilde{x}_1\ \tilde{x}_2\ \dots\ \tilde{x}_{F_s N}]^T = \tilde{\mathbf{A}}\boldsymbol{\omega} \tag{5}$$

where $\tilde{\mathbf{A}} = [\tilde{\mathbf{x}}_1\ \tilde{\mathbf{x}}_2\ \dots\ \tilde{\mathbf{x}}_U]$, $\tilde{\mathbf{x}}_u = \tilde{\mathbf{F}}^H \mathbf{s}_u$, and $\tilde{\mathbf{F}}$ is an $N \times F_s N$ matrix whose (k,l)th element is $\frac{\exp(-j2\pi(k-1)(l-1)/F_s N)}{\sqrt{N}}$. The PAPR of $\tilde{\mathbf{x}}$ is defined as

$$\text{PAPR} = \frac{\|\tilde{\mathbf{x}}\|_\infty^2}{E[|\tilde{x}_n|^2]} = \frac{\max_{1 \le n \le F_s N} |\tilde{x}_n|^2}{E[|\tilde{x}_n|^2]} \tag{6}$$

where $E[\cdot]$ denotes the expectation operator.

2.2 Receiver

At a receiver shown in Fig. 1(b), the received signal after removing the CP is represented by

$$\mathbf{r} = [r_1\ r_2\ \dots\ r_N]^T = \mathbf{H}_c \mathbf{x} + \mathbf{z} \tag{7}$$

where $\mathbf{H}_c$ denotes the circulant matrix composed of the channel impulse response and $\mathbf{z}$ is the noise component. The

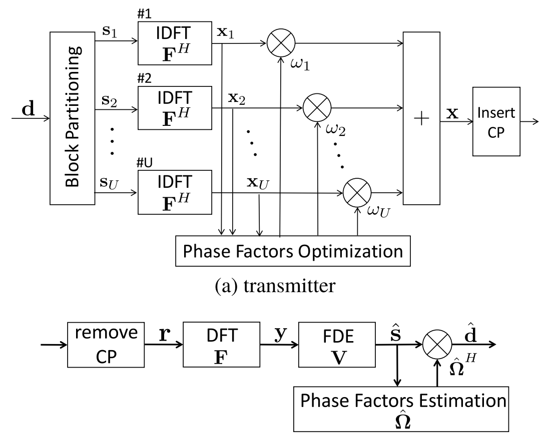

(a) transmitter

(b) receiver

Fig. 1 Block diagram of transmitter and receiver.

frequency-domain signal obtained by DFT is given by

$$\mathbf{y} = \mathbf{F}\mathbf{r} = \mathbf{F}\mathbf{H}_c\mathbf{x} + \mathbf{F}\mathbf{z} = \mathbf{F}\mathbf{H}_c\mathbf{F}^H\mathbf{S}\boldsymbol{\omega} + \mathbf{F}\mathbf{z}. \tag{8}$$

If the channel is known at the receiver, frequency-domain equalizer (FDE) outputs are represented by

$$\hat{\mathbf{s}} = [\hat{s}_1\ \hat{s}_2\ \dots\ \hat{s}_N]^T = \mathbf{V}\mathbf{y} = \mathbf{S}\boldsymbol{\omega} + \mathbf{V}\mathbf{F}\mathbf{z} \tag{9}$$

where $\mathbf{V} = (\mathbf{F}\mathbf{H}_c\mathbf{F}^H)^{-1}$ denotes an FDE matrix. Finally, we remove the effect of the phase factors to recover the data symbols as

$$\hat{\mathbf{d}} = \hat{\boldsymbol{\Omega}}^H \hat{\mathbf{s}} \tag{10}$$

where

$$\hat{\boldsymbol{\Omega}} = \begin{bmatrix} e^{j\hat{\theta}_1}\mathbf{1}_{N_b} & 0 & \cdots & 0 \\ 0 & e^{j\hat{\theta}_2}\mathbf{1}_{N_b} & \ddots & \vdots \\ \vdots & \ddots & \ddots & 0 \\ 0 & \cdots & 0 & e^{j\hat{\theta}_U}\mathbf{1}_{N_b} \end{bmatrix}, \tag{11}$$

$\hat{\theta}_u$ is an estimate of θ_u, and $\mathbf{1}_{N_b}$ is an $N_b \times 1$ vector with all-one elements.

Our purpose is twofold:

1) To determine $\boldsymbol{\omega}$ or $\boldsymbol{\theta} = [\theta_1\ \theta_2\ \dots\ \theta_U]^T$ at the transmitter such that the PAPR of $\tilde{\mathbf{x}}$ is reduced significantly;
2) To estimate $\boldsymbol{\omega}$ or $\boldsymbol{\theta}$ at the receiver without side information.

3. Optimization of Phase Factors

3.1 Conventional PTS-Based Methods

In the conventional PTS [5], a phase factor $\omega_u = e^{j\theta_u}$ is restricted to a finite set consisting of B discrete values, i.e., $\theta_u \in \{2\pi(k-1)/B \mid k = 1, 2, \cdots, B\}$ where B is the number of phase candidates (we refer to it as discrete-valued PTS (DPTS)). Since θ_1 can be fixed without any performance loss, there are B^{U-1} combinations of phase factors. We

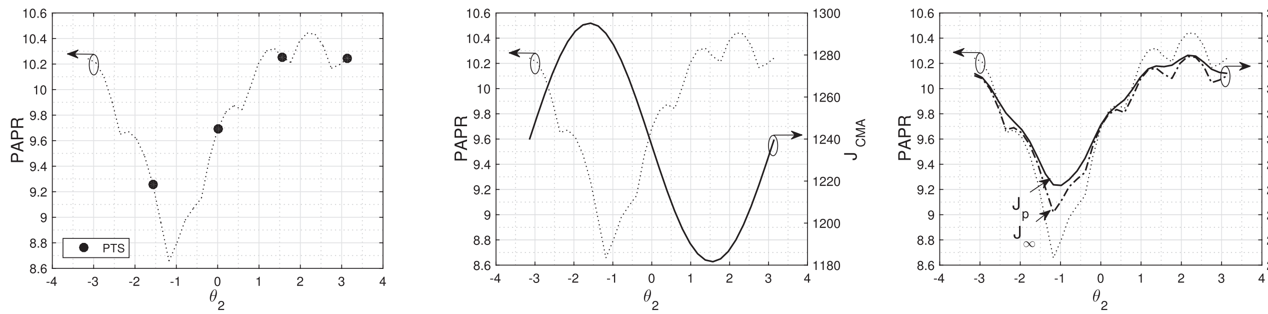

(a) DPTS (b) CMA (c) 32-norm and ∞-norm

Fig. 2 Example of PAPR and cost functions.

evaluate the PAPR of $\tilde{\mathbf{x}}$ for each combination, and select the optimum one which achieves the smallest PAPR. This exhaustive search requires a huge computational complexity which increases drastically as U or B increases.

Let us examine the advantage of continuous-valued phase factors over discrete-valued ones. We consider a simple example where $N = 256$, $F_s = 4$, and $U = 2$. In Fig. 2(a), an example of PAPR as a function of θ_2 is shown. Four plots on the curve are obtained by DPTS with $B = 4$. As can be seen, the minimum PAPR value cannot be achieved by DPTS. This example suggests that PAPR can be lowered by using continuous-valued phase factors.

The CMA-based method [11] determines continuous-valued phase factors such that the following cost function is minimized:

$$J_{\mathrm{CMA}}(\boldsymbol{\omega}) = \sum_{n=1}^{F_s N} (|\tilde{x}_n|^2 - \alpha)^2 \tag{12}$$

where α represents the average transmitted signal power. After the initialization of $\boldsymbol{\omega}^0$, the phase factors are updated by the following gradient descent method:

$$\bar{\boldsymbol{\omega}}^{i+1} = \boldsymbol{\omega}^i - \mu_{\mathrm{CMA}} \tilde{\mathbf{A}}^H \hat{\mathbf{s}}_e^i, \tag{13}$$

$$\boldsymbol{\omega}^{i+1} = \bar{\boldsymbol{\omega}}^{i+1} \oslash |\bar{\boldsymbol{\omega}}^{i+1}| \tag{14}$$

where $\hat{\mathbf{s}}_e^i = \hat{\mathbf{s}}^i \odot \mathbf{e}^i$, $\hat{\mathbf{s}}^i = \tilde{\mathbf{A}}\boldsymbol{\omega}^i$, $\mathbf{e}^i = (\hat{\mathbf{s}}^i \odot \hat{\mathbf{s}}^{i*}) - \alpha \mathbf{1}_{F_s N}$, μ_{CMA} is a step size parameter, $\odot$ represents the element-wise product, $\oslash$ represents the element-wise quotient, and $|\cdot|$ represents the element-wise absolute value. Unlike DPTS, its computational complexity does not increase exponentially with U and is independent of B.

Let us look at the previous example again. In Fig. 2(b), an example of the CMA cost function $J_{\mathrm{CMA}}(\theta_2)$ as a function of θ_2 is shown. As can be seen, the surface of $J_{\mathrm{CMA}}(\theta_2)$ is very smooth. However, the phase coefficient θ_2 corresponding to the minimum $J_{\mathrm{CMA}}(\theta_2)$ is different from that corresponding to the minimum PAPR. This motivates us to investigate cost functions other than $J_{\mathrm{CMA}}(\boldsymbol{\omega})$.

3.2 p-Norm Minimization

Since the average power $E[|\tilde{x}_n|^2]$ is constant, PAPR in (6) can be minimized by minimizing the infinity-norm of $\tilde{\mathbf{x}}$. An immediate idea is to employ the infinity-norm of $\tilde{\mathbf{x}}$ as the cost function:

$$J_\infty(\boldsymbol{\omega}) = \|\tilde{\mathbf{x}}\|_\infty = \max_n |\tilde{x}_n|. \tag{15}$$

Gradient descent methods for the infinity-norm minimization have been considered for the TR method in OFDM systems [16] and the SLM method in space shift keying OFDM systems [17]. As can be observed in Fig. 2(c), however, the infinity-norm cost function $J_\infty(\theta_2)$ is a non-smooth function and has multiple local minima. Then, gradient descent algorithms can get trapped in one of the undesired minima.

To overcome this issue, we consider the p-norm of $\tilde{\mathbf{x}}$ given by

$$J_p(\boldsymbol{\omega}) = \|\tilde{\mathbf{x}}\|_p = \sqrt[p]{\sum_{n=1}^{F_s N} |\tilde{x}_n|^p}. \tag{16}$$

Through some numerical examples, we have confirmed a tendency that $J_p(\theta_2)$ is smooth but its minimum is different from the minimum PAPR for too small p, and vice versa for too large p. In Fig. 2(c), an example of the cost function $J_p(\theta_2)$ with $p = 32$ is shown. It can be observed that the $J_p(\theta_2)$ is smooth, and the position of its minimum is almost coincident with that of the minimum PAPR. From this example, we can expect that a lower PAPR can be achieved by a gradient descent method of $J_p(\boldsymbol{\omega})$ with a properly chosen value of p.

Now, we derive an iterative gradient descent algorithm for $J_p(\boldsymbol{\omega})$ minimization. We consider the direct update of the phase coefficients $\boldsymbol{\theta}$ rather than the phase factors $\boldsymbol{\omega}$. The gradient of $J_p(\boldsymbol{\theta})$ with respect to $\boldsymbol{\theta}$ is given by

$$\frac{\partial J_p(\boldsymbol{\theta})}{\partial \boldsymbol{\theta}} = 2\Re\left[j \left(\sum_{n=1}^{F_s N} |\tilde{x}_n|^p \right)^{\frac{1-p}{p}} \left(\sum_{n=1}^{F_s N} \tilde{x}_n^* |\tilde{x}_n|^{p-2} \tilde{\mathbf{a}}_n^* \right) \odot \boldsymbol{\omega} \right] \tag{17}$$

where $\tilde{\mathbf{a}}_n^H$ denotes the nth row of $\tilde{\mathbf{A}}$ and $\Re[\cdot]$ represents the real part of a complex number. Then, the updating equation is written by

$$\boldsymbol{\theta}^{i+1} = \boldsymbol{\theta}^i - \mu_p \frac{\partial J_p(\boldsymbol{\theta})}{\partial \boldsymbol{\theta}}$$

$$= \boldsymbol{\theta}^i - \mu_p \Re\left[j\left(\sum_{n=1}^{F_sN} |\tilde{x}_n^i|^p\right)^{\frac{1-p}{p}} \left(\sum_{n=1}^{F_sN} \tilde{x}_n^{i*}|\tilde{x}_n^i|^{p-2}\tilde{\mathbf{a}}_n^*\right) \odot \boldsymbol{\omega}^i \right] \quad (18)$$

where $\boldsymbol{\omega}^i = [e^{j\theta_1^i} \ \ldots \ e^{j\theta_U^i}]^T$, $\tilde{x}_n^i = \tilde{\mathbf{a}}_n^H \boldsymbol{\omega}^i$, and μ_p is a step size parameter.

For reference purpose, we derive an iterative algorithm for $J_\infty(\boldsymbol{\theta})$ minimization. Since the gradient of $J_\infty(\boldsymbol{\theta})$ is difficult to obtain directly, we approximate it by the limit of the gradient of p-norm as [16], [17]

$$\frac{\partial J_\infty(\boldsymbol{\theta})}{\partial \boldsymbol{\theta}} = \lim_{p\to\infty} \frac{\partial J_p(\boldsymbol{\theta})}{\partial \boldsymbol{\theta}} = \Re\left[j\tilde{x}_b^* |\tilde{x}_b|^{-1} \tilde{\mathbf{a}}_b^* \odot \boldsymbol{\omega} \right] \quad (19)$$

where $b = \arg\max_n |\tilde{x}_n|$. Then, the updating equation can be written as

$$\boldsymbol{\theta}^{i+1} = \boldsymbol{\theta}^i - \mu_\infty \Re\left[j\tilde{x}_b^{i*} |\tilde{x}_b^i|^{-1} \tilde{\mathbf{a}}_b^* \odot \boldsymbol{\omega}^i \right] \quad (20)$$

where μ_∞ is a step size parameter.

3.3 Proposed PAPR Reduction Method

At the receiver, the knowledge of $\boldsymbol{\theta}$ is required to remove the effect of phase rotation by $\boldsymbol{\theta}$. To get the knowledge of $\boldsymbol{\theta}$, it is undesirable to use SI or pilot symbols, which waste bandwidth. If $\boldsymbol{\theta}$ is determined according to (18) and is allowed to take any value in $[0, 2\pi]$, it is impossible to estimate $\boldsymbol{\theta}$ at the receiver without SI or pilot symbols.

To overcome this issue, we propose to limit the range of $\boldsymbol{\theta}$ to identify $\boldsymbol{\theta}$ uniquely at the receiver. More specifically, θ_u is allowed to take a value in $(-\theta_{\lim}, +\theta_{\lim})$. The choice of $\theta_{\lim} > 0$ affects both the PAPR characteristic and the BER performance. The influence of $\theta_{\lim}$ is discussed later. The procedure of the proposed method is summarized as follows:

Step 1) Set the initial value $\boldsymbol{\theta}^0$ to zero.
Step 2) Update $\boldsymbol{\theta}^i$ by (18).
Step 3) Round θ_u^i taking a value outside the range $(-\theta_{\lim}, +\theta_{\lim})$ down(up) to $\theta_{\lim}(-\theta_{\lim})$ as follows:

$$\theta_u^i = \begin{cases} \theta_u^i, & -\theta_{\lim} \le \theta_u^i \le +\theta_{\lim} \\ -\theta_{\lim}, & \theta_u^i < -\theta_{\lim} \\ +\theta_{\lim}, & \theta_u^i > +\theta_{\lim} \end{cases}. \quad (21)$$

Step 4) Repeat Step 2) and Step 3) until the preset number of iterations I.

3.4 Computational Complexity

Let us consider the computational complexity required to determine $\boldsymbol{\theta}$ at the transmitter. The number of complex multiplications required by DPTS C_{DPTS} and that by the proposed method C_p are given by

$$C_{\mathrm{DPTS}} = B^{U-1}UF_sN + B^{U-1}F_sN, \quad (22)$$
$$C_p = \{(2U + q + 1)F_sN + 2U + 2\}I \quad (23)$$

Table 1 Computational complexity comparison.

U	C_{DPTS}	C_p
4	6.5×10^4	1.4×10^6
8	1.7×10^7	2.3×10^6
16	1.1×10^{12}	3.9×10^6
32	4.7×10^{21}	7.2×10^6
64	8.7×10^{40}	1.4×10^7

where $p = 2^q$. In (22), the first and second terms are required to generate B^{U-1} phase factor candidates and to evaluate the PAPR in (6), respectively. Note that the computation corresponding to the first term can be avoided for $B \le 4$ or be reduced for $B > 4$ by IQ swapping and sign inversion if θ_u takes a value in the set $\{\frac{2\pi(m-1)}{B}, m = 1, \ldots, B\}$ where $B = 2^b$ and b is a positive integer. Table 1 compares C_{DPTS} and C_p where $N = 256$, $B = 4$, $I = 100$, $q = 5$ ($p = 32$), and the first term in (22) is ignored. It can be observed that the complexity of the proposed method almost increases linearly with the number of RB U, whereas that of DPTS increases exponentially.

4. Blind Estimation of Continuous Phase Factors

4.1 QPSK

We propose a method to blindly estimate a phase coefficient θ_u (equivalently, phase factor $\omega_u = e^{j\theta_u}$) for QPSK modulation with constellation points $s_i, i = 1, 2, 3, 4$. The basic idea is to estimate θ_u from the difference between an FDE output and its closest constellation point.

Assuming that the channel is known at the receiver, the FDE outputs of the uth RB are given by

$$\hat{s}_{(u-1)N_b+n_b} = e^{j\theta_u} s_{u,n_b} + w_{u,n_b} \quad (24)$$

for $n_b = 1, 2, \cdots, N_b$, where w_{u,n_b} is a noise component. Fig. 3 shows an example. Suppose that s_1 is the transmitted data symbol, i.e., $s_{u,n_b} = s_1$. In the absence of the channel noise (a), the closest point to the FDE output $\hat{s}_{(u-1)N_b+n_b}$ is s_1 if $\theta_{\lim}$ satisfies

$$\theta_{\lim} \le \pi/4. \quad (25)$$

Then, the phase difference $\hat{\theta}_{u,n_b}$ between $\hat{s}_{(u-1)N_b+n_b}$ and s_1 is identical to θ_u. In noisy situations as shown in Fig. 3(b), $\hat{\theta}_{u,n_b}$ is not identical to θ_u. Thus, we get a final estimate by averaging $\hat{\theta}_{u,n_b}$ over N_b symbols in the uth RB. The estimation procedure is summarized as follows:

Step 1) Find the closest constellation point to an FDE output $\hat{s}_{(u-1)N_b+n_b}$ for $n_b = 1, 2, \cdots, N_b$ as follows:

$$\hat{p}_{u,n_b} = \arg\min_p |\hat{s}_{(u-1)N_b+n_b} - s_p|. \quad (26)$$

Step 2) Obtain the phase difference between the FDE output and its closest constellation point:

$$\hat{\theta}_{u,n_b} = \arg(\hat{s}_{(u-1)N_b+n_b}) - \arg(s_{\hat{p}_{u,n_b}}). \quad (27)$$

Step 3) Obtain the phase coefficient estimate of the uth RB

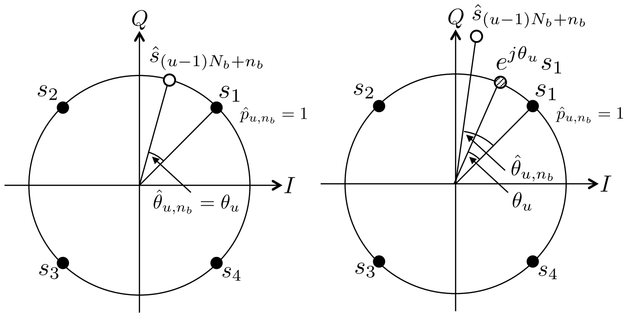

(a) noiseless case (b) noisy case

Fig. 3 Example of phase estimation for QPSK where s_1 is the transmitted symbol. (a) noiseless estimate $\hat{\theta}_{u,n_b}$ is equal to θ_u if $\theta_{\rm lim} < \pi/4$. (b) noisy estimates $\hat{\theta}_{u,n_b}$ are different from θ_u and are refined by averaging them.

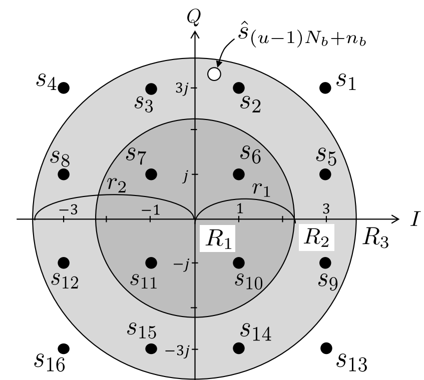

Fig. 4 Decision region for 16QAM where filled circles denote constellation points and the open circle denotes an example of an FEQ output.

$\hat{\theta}_u$ by averaging $\hat{\theta}_{u,n_b}$ over N_b symbols in the uth RB:

$$\hat{\theta}_u = \frac{1}{N_b}\sum_{n_b=1}^{N_b}\hat{\theta}_{u,n_b}. \tag{28}$$

Since the phases coefficients are estimated in a decision directed manner in (27), it is desirable that there are a few errors on the tentative data decision in (26). To prevent the tentative decision error, $\theta_{\rm lim}$ should be small. However, PAPR cannot be lowered for small $\theta_{\rm lim}$. Thus, $\theta_{\rm lim}$ should be determined by taking into account the trade-off between BER and PAPR. It is noted that even if there are a few erroneous tentative decisions, the estimation result is acceptable due to the averaging in (28). Actually, our preliminary simulations (not shown here) have shown that the BER performance of the proposed method is superior to that obtained by the tentative decision (26) without Steps 2 and 3.

The proposed method can also be applied to BPSK modulation. In this case, the condition (25) is replaced by $\theta_{\rm lim} \le \pi/2$. Similarly, the procedure can be applied to M-ary PSK by setting $\theta_{\rm lim} \le \pi/M$. However, since the range $(-\theta_{\rm lim}, \theta_{\rm lim})$ becomes narrow for large M, PAPR cannot be lowered significantly. A modified method for 16QAM shown in the next subsection can be applied to such cases.

The receiver requires the knowledge of the channel. Channel estimation methods using pilot symbols are commonly used, but they do not work in PTS-based systems. Because they cannot distinguish between the phase rotation by the channel and that by PTS. On the other hand, blind channel estimation methods such as [18] work since they are not affected by the phase rotation due to PTS. Thus, throughout the paper, we can assume the perfect channel knowledge at the receiver.

4.2 16QAM

When the proposed estimation method is applied to 16QAM, it is anticipated that the PAPR performance becomes poor because $\theta_{\rm lim}$ is very restricted. To resolve this issue, we modify the estimation method. The basic idea of the modified method is as follows: $\theta_{\rm lim}$ is allowed to take a value in (25) to ensure a low PAPR characteristic; and not only the closest constellation point but also the second closest point is taken into consideration for phase estimation.

Let us consider the 16QAM modulation where constellation points are $\{\pm1\pm j, \pm1\pm3j, \pm3\pm3j, \pm3\pm j\}$. We define decision regions of an FDE output $\hat{s}_i$ as shown in Fig. 4:

$$R_1:\ |\hat{s}_i| < r_1$$
$$R_2:\ r_1 < |\hat{s}_i| < r_2$$
$$R_3:\ |\hat{s}_i| > r_2$$

where $r_1 = (\sqrt{2}+\sqrt{10})/2 = 2.2882$ and $r_2 = (\sqrt{10}+\sqrt{18})/2 = 3.7025$[†]. We denote the region where an FDE output $\hat{s}_{(u-1)N_b+n_b}$ falls in as R_{u,n_b}. For example, $R_{u,n_b} = R_2$ if $\hat{s}_{(u-1)N_b+n_b}$ is in the region R_2. The modified phase estimation procedure for θ_u is summarized as follows:

Step 1) Find the region R_{u,n_b} for $n_b = 1, 2, \cdots, N_b$.
Step 2) Find the closest constellation point $\hat{p}_{u,n_b,1}$ in R_{u,n_b} to $\hat{s}_{(u-1)N_b+n_b}$ in the same way as (26). In addition, if $R_{u,n_b} = R_2$, find the second closest point $\hat{p}_{u,n_b,2}$ in R_2.
Step 3) Obtain the phase difference $\hat{\theta}_{u,n_b,1}$ between $\hat{s}_{(u-1)N_b+n_b}$ and $s_{\hat{p}_{u,n_b,1}}$ in the same way as (27). In addition, if $R_{u,n_b} = R_2$, obtain the phase difference $\hat{\theta}_{u,n_b,2}$ for the second closest point.
Step 4) Suppose that N_2 out of N_b FDE outputs fall in R_2. Then, there are 2^{N_2} combinations of N_b phase differences $\{\hat{\theta}_{u,n_b,i}\}$. For the kth combination, set the phase difference of the n_bth symbol $\hat{\theta}^{(k)}_{u,n_b}$ to $\hat{\theta}_{u,n_b,1}$ if $R_{u,n_b} = R_1$ or R_3, or set $\hat{\theta}^{(k)}_{u,n_b}$ to $\hat{\theta}_{u,n_b,1}$ or $\hat{\theta}_{u,n_b,2}$ if $R_{u,n_b} = R_2$.
Step 5) Obtain the average $\hat{\theta}^{(k)}_u$ of $\hat{\theta}^{(k)}_{u,n_b}$ for $k = 1, 2, \cdots, 2^{N_2}$, in the same way as (28).
Step 6) Determine the final estimate $\hat{\theta}_u = \hat{\theta}^{(\hat{k})}_u$ where

[†] r_1 is chosen such that the circle centered at the origin with the radius of r_1 is in the middle of the circle passing through s_6 with the radius of $\sqrt{2}$ and the circle passing through s_2 with the radius of $\sqrt{10}$. r_2 is chosen in the same way.

$$\hat{k} = \arg\min_{k} \frac{1}{N_b} \sum_{n_b=1}^{N_b} \left(\hat{\theta}_u^{(k)} - \hat{\theta}_{u,n_b}^{(k)}\right)^2. \quad (29)$$

The idea behind of (29) is that we choose the phase combination with the minimum variance within an RB because if the tentative decision in Step 2) is correct the phase difference is small.

4.3 Computational Complexity

Let us evaluate the computational complexity for phase estimation at the receiver. First, we consider the QPSK case described in 4.1. The numbers of complex multiplications in each Step are $C_1^\times = 4N$, $C_2^\times = N$, and $C_3^\times = U$, respectively. The total number of multiplications is $C_{QPSK}^\times = 5N + U$. Next, we consider the 16QAM case shown in 4.2. The numbers of complex multiplications in each Step are $C_1^\times = N$, $C_2^\times = 4N + 4N_2$, $C_3^\times = N + N_2$, $C_4^\times = 0$, $C_5^\times = 2^{N_2}U$, and $C_6^\times = 2^{N_2}N_bU$, respectively. The total number of multiplications is $C_{16QAM}^\times = 6N + 5N_2 + 2^{N_2}(U + N)$. The computational complexity can increase exponentially in the case of 16QAM.

In the conventional pilot-based phase estimation methods [13], [15], their computational complexity, which is proportional to U, does not depend on modulation schemes. Unlike the proposed blind method, however, they waste bandwidth due to the transmission of pilot symbols.

5. Simulation Results

Unless otherwise stated, the parameters used in the simulation are as follows: the number of subcarriers $N = 256$, oversampling factor $F_s = 4$, the number of RB $U = 8$ (DPTS), 32 (CMA, proposed method), the number of phase candidates of DPTS $B = 4$, the number of iterations $I = 100$, CP length $P = 64$, and $p = 32$. The phase limitation $\theta_{\lim}$ is parameterized as $\theta_{\lim} = \pi/4 \times R$ where $R \in (0, 1]$ is the limiting factor and its default value was $R = 1.0$. We considered quasi-static Rayleigh fading channels of order $L = 10$ where channel taps were modeled as complex Gaussian random variables. Modulation scheme was QPSK. The step sizes were chosen such that the fastest convergence is achieved. We set the initial value of the phase coefficients θ_u^0 to zero†.

First, we show the performance of continuous-valued PTS methods when the range of $\boldsymbol{\theta}$ is unlimited. Figure 5 shows complementary cumulative distribution functions (CCDF) of the CMA-based method [11], the p-norm based method, and the infinity-norm based method. The performances of the continuous-valued PTSs are better than that of the conventional discrete-valued PTS (DPTS). Especially, the p-norm based method provides the best performance.

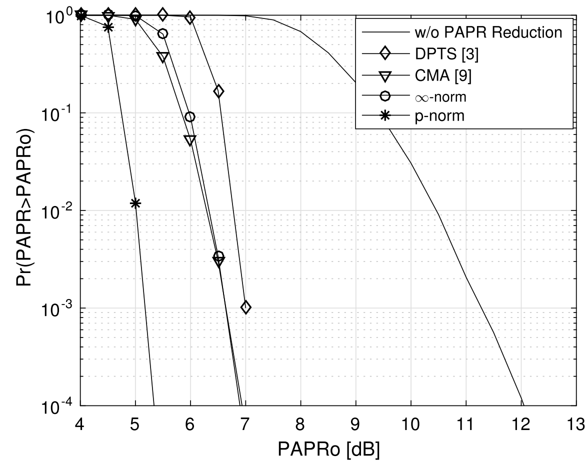

Fig. 5 CCDF by various PTS methods without phase limitation.

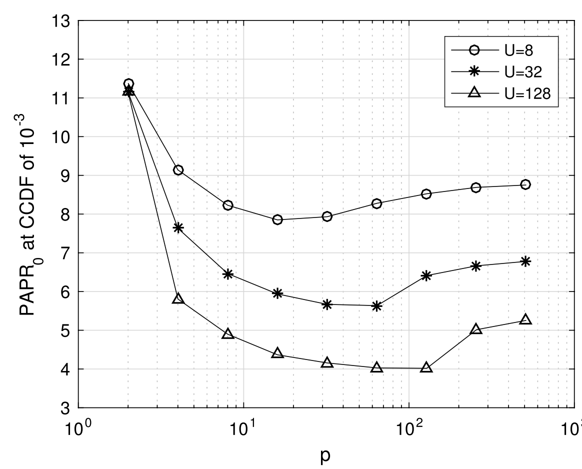

Fig. 6 Effect of p on PAPR performance.

This result supports the intuitive argument in Sect. 3.

In Fig. 6, the effect of p on PAPR performance of the proposed method is shown. The vertical axis represents the PAPR which achieves CCDF of 10^{-3}, i.e., $\Pr(\text{PAPR} > \text{PAPR}_0) = 10^{-3}$. We can observe that the PAPR performance depends on p. As mentioned in 3.2, from our preliminary simulation results, we have confirmed that the position of the minimum of the cost function is different from the position of the minimum PAPR when p is small. Also, we have found that the cost function has undesired local minima when p is large. On the other hand, as can be seen in Fig. 2(c), undesired local minima vanish, and the minimum of the cost function is coincident with the minimum PAPR for moderate p. Actually, it is seen from Fig. 6 that the best value of p depends on U, and low PAPR can be achieved by setting p between 10 to 100.

The effect of the number of RB U on PAPR is shown in Fig. 7. The results of DPTS for $U > 8$ cannot be obtained due to extremely long computational time. As shown in Table 1, the computational complexity of DPTS with $U = 8$ is almost the same as that of the proposed method with $U = 64$. Then, we can observe from Fig. 7 that the PAPR achieved by DPTS

†We tried other initial values and obtained the same performance for the proposed p-norm based method with $p = 32$. Unfortunately, the convexity of the cost function J_p is not ensured. Nevertheless, the initial value issue seems not to be serious by choosing p carefully.

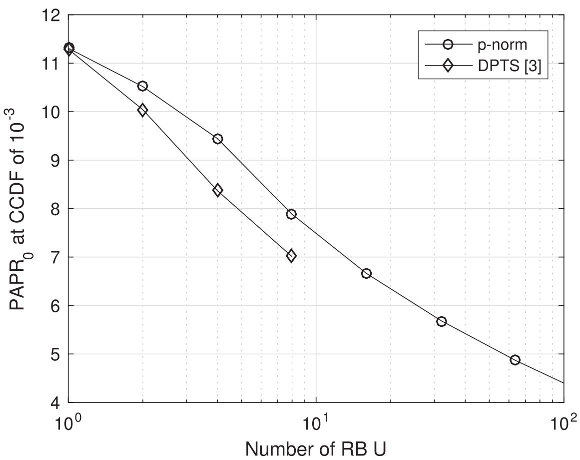

Fig. 7 Effect of the number of RB U on PAPR.

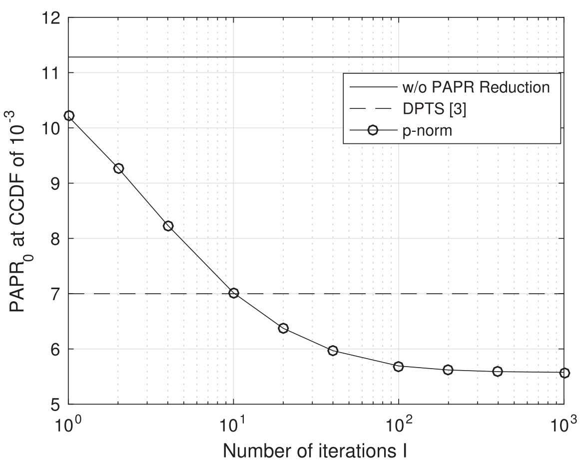

Fig. 8 PAPR convergence performance.

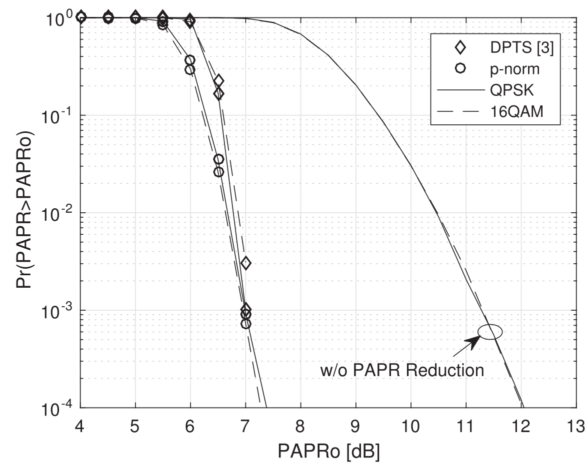

Fig. 9 CCDF for QPSK and 16QAM.

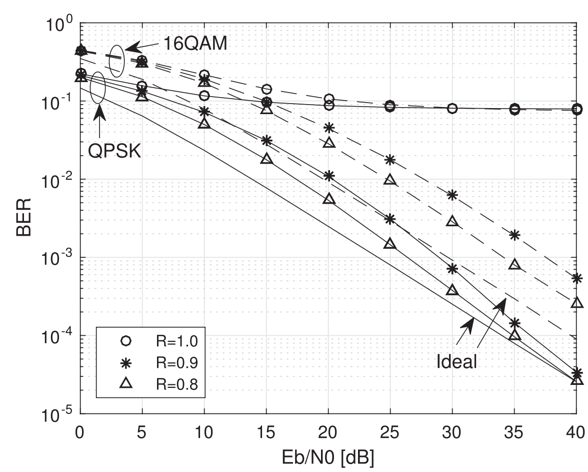

Fig. 10 BER performance for QPSK and 16QAM.

with $U = 8$ is higher than that by the proposed method with $U = 64$. Note that this observation does not mean that DPTS is always inferior to the proposed method. When $U = 4$, DPTS is simpler than the proposed method, and its PAPR is lower than that of the proposed method. For small U, DPTS has advantages over the proposed method although its achievable PAPR is not low enough. The proposed method still works for $U > 8$ since its computational complexity is significantly low, and its PAPR decreases as U increases. For large U, the proposed method is advantageous in both complexity and PAPR performance.

Figure 8 shows the PAPR convergence curve. It is seen that the proposed method achieves the PAPR of 7 dB obtained by DPTS with a few iterations, say $I = 10$. Also, the proposed method can be superior to DPTS if more iterations are allowed.

In Fig. 9, CCDFs of the DPTS and the proposed method are shown for QPSK and 16QAM. The number of iterations I was set such that the proposed method achieves CCDF of 10^{-3} at PAPR$_0$ of 7 dB. The PAPR performance of the proposed method with $U = 32$ is almost the same as that of DPTS with $U = 8$. Note that the computational complexity of the proposed method with $U = 32$ is lower than that of DPTS with $U = 8$ as shown in Table 1.

Figure 10 illustrates the BER performances of the proposed method for QPSK and 16QAM. We assumed the use of a solid state power amplifier (SSPA) with AM/AM conversion characteristics $g(x) = x/[1 + (\frac{x}{A})^{2\rho}]^{\frac{1}{2\rho}}$ where x is the amplitude of input signal, A is the output saturation level and the parameter ρ controls the smoothness. We set $\rho = 2$. To reduce nonlinear distortion in the output signal, the input back off was set 7 dB. The performance of the ideal case with no distortion is also shown. The performance of the proposed method with $R = 1.0$ ($\theta_{\lim} = \pi/4$) is poor because the tentative data decision in (26) is susceptible to the channel noise. As R decreases ($\theta_{\lim}$ decreases), the performance improves for both QPSK and 16QAM due to insusceptibility to the channel noise.

We show the PAPR performance for various R in Fig. 11. Unlike the BER performance in Fig. 10, the PAPR performance degrades as the limiting factor R decreases because the phase factors should be taken from a narrower range. To explicitly examine the trade-off between the BER

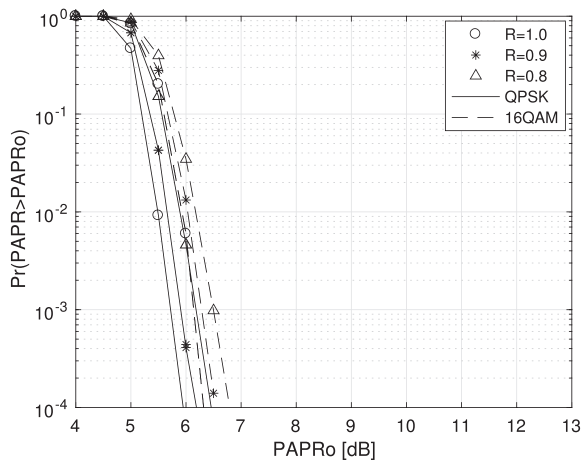

Fig. 11 CCDF for various limiting factor R.

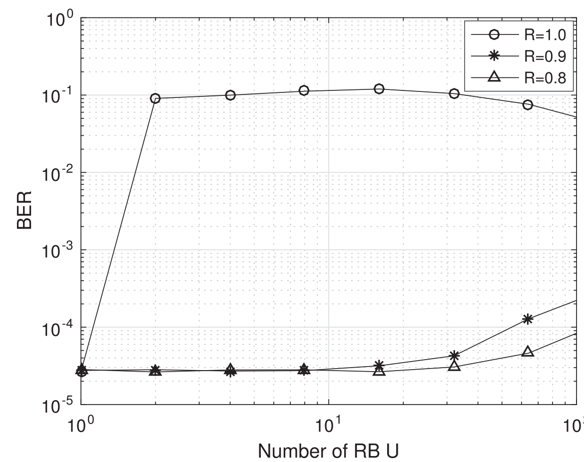

Fig. 13 Effect of the number of RB U on BER.

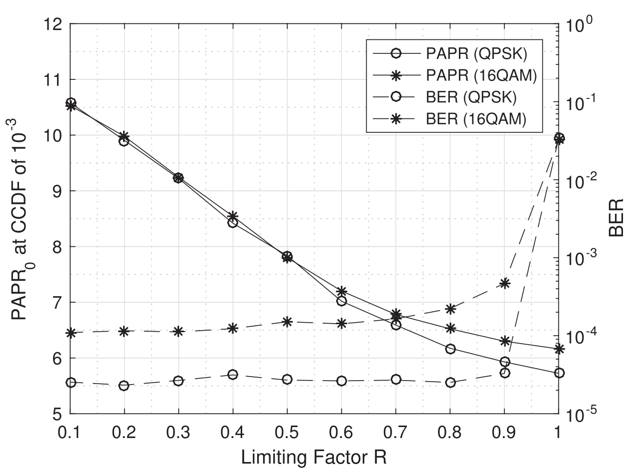

Fig. 12 Effect of the limiting factor R on PAPR and BER.

performance and the PAPR reduction performance, both performances are shown for a wider range of R in Fig. 12 where $E_b/N_0 = 40$ dB. In practice, R is chosen by taking into account the tradeoff between BER and PAPR. In this example, $R = 0.8$ might be a good choice because the BER degradation is not serious if $R \leq 0.8$ and the PAPR degradation is less than 1 dB if $R \geq 0.8$.

Figure 13 shows the effect of the number of RB U on BER where E_b/N_0=40 dB. For $R < 1.0$, the performance improves as U decreases because then N_b increases and the averaging in (28) is more effective. For $R = 1.0$, the averaging is not effective anymore due to undesirable tentative data decision errors.

6. Conclusion

In this paper, we proposed a PAPR reduction method based on p-norm minimization. It was shown that the proposed method can achieve the desired PAPR characteristic by determining continuous-valued phase factors with small computational load even if the number of RB is large. In addition, we proposed a phase factor estimation method without SI and pilot symbols. It was shown that the proposed methods can provide satisfactory BER performance by limiting the range of the phase factors properly.

Unfortunately, it is not easy to apply the proposed phase estimation method to higher order QAM. Because the estimation procedure becomes complicated and the computational complexity increases as the number of decision regions increases. It is important to overcome this problem for low-cost implementation of OFDM-based high-speed communication systems. Moreover, it is worth studying the convergence analysis and the initial value setting issue.

References

[1] S.H. Han and J.H. Lee, "An overview of peak-to-average power ratio reduction techniques for multicarrier transmission," IEEE Trans. Wireless Commun., vol.12, pp.56–65, April 2005.

[2] Y. Rahmatallah and S. Mohan, "Peak-to-average power ratio reduction in OFDM systems: A survey and taxonomy," IEEE Commun. Surveys Tuts., vol.15, no.4, pp.1567–1592, March 2013.

[3] J. Tellado and J.M. Cioffi, "Peak power reduction for multicarrier transmission," Proc. IEEE CTMC GLOBECOM'98, pp.219–224, Sydney, Australia, Nov. 1998.

[4] R.W. Bauml, R.F.H. Fisher, and J.B. Huber, "Reducing the peak-to-average power ratio of multicarrier modulation by selected mapping," Electron. Lett., vol.32, no.22, pp.2056–2057, Oct. 1996.

[5] S.H. Müller and J.B. Huber, "A novel peak power reduction scheme for OFDM," Proc. 1997 IEEE 8th Int. Symp. on Personal, Indoor and Mobile Radio Commun. (PIMRC), pp.1090–1094, 1997.

[6] L.J. Cimini, Jr. and N.R. Sollenberger, "Peak-to-average power ratio reduction of an OFDM signal using partial transmit sequences," IEEE Commun. Lett., vol.4, no.3, pp.86–88, March 2000.

[7] S.H. Han and J.H. Lee, "PAPR reduction of OFDM signals using a reduced complexity PTS technique," IEEE Signal Process. Lett., vol.11, no.11, pp.887–890, Nov. 2004.

[8] N. Taspinar, A. Kalinli, and M. Yildirim, "Partial transmit sequences for PAPR reduction using parallel tabu search algorithm in OFDM systems," IEEE Commun. Lett., vol.15, no.9, pp.974–976, Sept. 2011.

[9] C. Tellambura, "Improved phase factor computation for the PAR reduction of an OFDM signal using PTS," IEEE Commun. Lett., vol.5, no.4, p.135–137, April 2001.

[10] E. Hong, H. Kim, and D. Har, "PAPR reduction by a single adaptive all-pass filter for OFDM systems," IEICE Electron. Express, vol.8,

no.19, pp.633–1639, Oct. 2011.
[11] S. Khademi and A.-J. van der Veen, "Constant modulus algorithm for peak-to-average power ratio (PAPR) reduction in MIMO OFDM/A," IEEE Signal Process. Lett., vol.20, no.5, pp.531–534, May 2013.
[12] M. Breiling, S.H. Müller, and J.B. Huber, "SLM peak-power reduction without explicit side information," IEEE Commun. Lett., vol.5, no.6, pp.239–241, June 2001.
[13] T. Fujii and M. Nakagawa, "Weighting factor estimation methods for partial transmit sequences OFDM to reduce peak power," IEICE Trans. Commun., vol.E85-B, no.1, pp.221–230, Jan. 2002.
[14] A.D.S. Jayalath and C. Tellambura, "SLM and PTS peak-power reduction of OFDM signals without side information," IEEE Trans. Wireless Commun., vol.4, no.5, pp.2006–2013, Sept. 2005.
[15] L. Guan, T. Jiang, D. Qu, and Y. Zhou, "Joint channel estimation and PTS to reduce peak-to-average-power ratio in OFDM systems without side information," IEEE Signal Process. Lett., vol.17, no.10, pp.883–886, Oct. 2010.
[16] S. Janaaththanan, C. Kasparis, and B.G. Evans, "A gradient based algorithm for PAPR reduction of OFDM using tone reservation technique," Proc. 2008 IEEE Veh. Technol. Conf. (VTC)-Spring, pp.2977–2980, Singapore, May 2008.
[17] P. Yang, Y. Xiao, and S. Li, "An improved gradient-based PAPR reduction method for space shift keying (SSK)-OFDM systems," IEICE Trans. Commun., vol.E94-B, no.12, pp.3532–3539, Dec. 2011.
[18] H. Wang, Y. Lin, and B. Chen, "Data-efficient blind OFDM channel estimation using receiver diversity," IEEE Trans. Signal Process., vol.51, no.10, pp.2613–2623, Oct. 2003.

Moeko Yoshida received the B.Eng. and M.Eng. degrees in electrical and electronic engineering from Ibaraki University, Hitachi, Japan in 2015 and 2017, respectively. In 2017, she joined JVCKENWOOD Engineering Corp., Yokohama, Japan. Her research interests include signal processing for wireless communications.

Hiromichi Nashimoto received the B.Eng. and M. Eng. degrees in electrical and electronic engineering from Ibaraki University, Hitachi, Japan in 2013 and 2015, respectively. In 2015, he joined Nippon Signal Co. Ltd. His research interests include signal processing for wireless communications.

Teruyuki Miyajima received the B.Eng., M.Eng., and Ph.D. degrees in electrical engineering from Saitama University, Saitama, Japan, in 1989, 1991, and 1994, respectively. In 1994, he joined Ibaraki University, Hitachi, Japan, where he is currently a professor in the Department of Electrical and Electronic Engineering. His current interests are in signal processing for wireless communications. Dr. Miyajima is a member of IEEE.